Colloids and Surfaces A: Physicochem. Eng. Aspects 511 (2016) 180–189

Contents lists available at ScienceDirect

Colloids and Surfaces A: Physicochemical and Engineering Aspects

journal homepage: www.elsevier.com/locate/colsurfa

# How asymmetric surfaces induce directional droplet motion

Nikolaos T. Chamakos, George Karapetsas, Athanasios G. Papathanasiou *

*School of Chemical Engineering, National Technical University of Athens, 15780, Greece*

## HIGHLIGHTS

- Mechanisms of droplet motion on asymmetrically patterned substrates.
- How vibrations induce directional droplet motion.
- Effect of solid surface geometry features on droplet velocity.
- Prediction of contact angle hysteresis and droplet speed.

## GRAPHICAL ABSTRACT

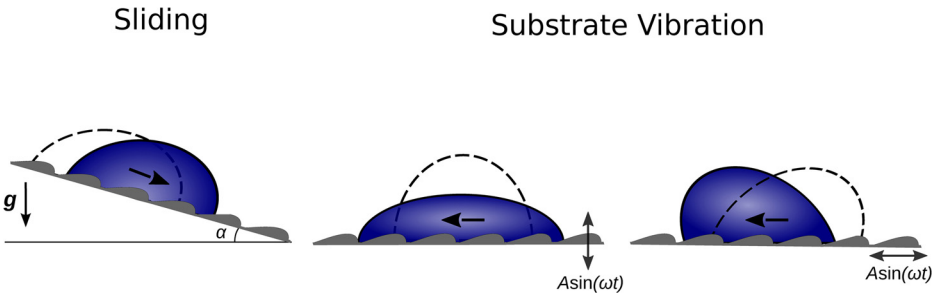


## ARTICLE INFO

*Article history:*
Received 13 April 2016
Received in revised form
19 September 2016
Accepted 23 September 2016
Available online 24 September 2016

*Keywords:*
Droplet dynamics
Anisotropic wettability
Contact line motion
Substrate vibration

## ABSTRACT

Asymmetrically patterned surfaces appear in many living organisms. An intriguing example is the ratchet-like structures of the *Morpho aega* butterfly wings which help to keep water droplets away from the body of the insect, thus enhancing the flying stability. Here, we investigate the mechanisms of droplet motion on asymmetrically structured substrates and predict conditions that favor preferential droplet transport. To this end, we present a numerical investigation of the droplet dynamics on hydrophobic surfaces. Crucially, our model is able to handle the possibility of air inclusions in the structure of the solid surface (e.g. droplets in Cassie state). Our results indicate that the unbalanced capillary force, developed at the contact line, is the key factor for achieving a preferable liquid motion direction. Thus, a sliding droplet on an asymmetrically structured surface exhibits different migration velocities depending on the direction of the structures with respect to the motion, only when the capillary forces are predominant against the effect of inertia (e.g. this behavior is not observed for a fluid with low surface tension). We also show that the anisotropic wetting properties, due to the structure asymmetry, can be exploited in order to passively transfer a droplet by vibrating the substrate, either vertically or horizontally. A parametric study is presented, varying the vibration amplitude as well as the length scale of the asymmetric roughness to demonstrate the effect of these factors on the migration velocity of the droplet.



## 1. Introduction

Engineering the wettability of solid materials, by means of fabricating surface micro-textures, has attracted the interest of many researchers over the past years [1–3]. In particular, surface patterning enables to transform a hydrophobic material into highly water-repellent (super-hydrophobic surface). A droplet on such an artificially roughened substrate behaves like a "liquid sphere" which can easily roll off in any direction. The above behavior is extremely useful for manipulating droplets in micro-devices, under an external actuation (e.g. lab-on-a-chip [4], fuel cells [5]). The selection of the optimal actuation type for handling a sessile droplet in such micro-devices has been extensively studied. Several techniques have been proposed like the electrowetting effect [6], thermocapillary convection [7], the Leidenfrost phenomenon [8] and acoustic fields [9]. In addition, droplet handling can be achieved

* Corresponding author.
*E-mail address:* pathan@chemeng.ntua.gr (A.G. Papathanasiou).

http://dx.doi.org/10.1016/j.colsurfa.2016.09.078
0927-7757/

by a combination of vertical and horizontal substrate vibrations which result, due to their phase difference, in the breaking of the droplet axial symmetry [10–13]. Recently, researchers have also demonstrated that the uni-directional droplet transport can be facilitated on surfaces featuring anisotropic wettability (with asymmetric micro-structures), even if the micro-device is operating under non-stationary conditions [14–17]. The latter case actually requires only one driving oscillation, since the symmetry breaking occurs due to the anisotropy of the solid substrate.

The concept of fabricating surfaces with anisotropic wettability originates from living organisms. In particular, Zheng et al., in a milestone work [18], found that the wings of the Morpho aega butterfly are covered by asymmetric ratchet-like structures enabling a droplet to exhibit both rolling and pinning behavior under different directions. The above characteristic drives the water away from the wings (and not toward its body) in a humid environment, providing flying stability for the butterfly. A plethora of similar structure morphologies, that can directionally control the movement of droplets, have been also discovered in living nature (e.g. shark and lizard skin, spider silk) [19–21], inspiring the design of asymmetrically structured substrates in order to handle small amounts of liquid [22–26].

Determining the preferable motion direction on an asymmetrically patterned surface is, however, still an ambiguous issue in the literature, since it is affected by the local forces applied in the vicinity of the contact line. In particular, different motion directions of droplets on asymmetrically structured, vibrating substrates were considered in published experiments [15] and simulations [17]. Furthermore, despite the fact that a relation between the droplet velocity and oscillation amplitude is fundamental when designing microfluidic applications, it is a still a controversial issue since both linear [27] and non-linear [15] behaviors have been reported in the literature. From the above it is clear that different driving forces may exist, originating from competing mechanisms. Specifically, a droplet moves to the direction toward the corrugations tilt on the butterfly wings [28] whereas it self-propels to the opposite direction when deposited on a hot ratchet due to the vapor escape below the droplet (Leidenfrost phenomenon [8]).

The dynamic modeling, using continuum-level approaches, of a droplet moving on such complex substrates is tedious due to the contentious issue of the boundary condition imposed at the contact line (where the three different phases meet). In particular, an *a priori* unknown number of contact lines can be created due the presence of air inclusions trapped between the liquid and the solid. In order to tackle the above limitation, we have recently presented a sharp-interface, continuum-level formulation where the liquid–vapor and the liquid–solid interfaces are treated in a unified context (one equation for both interfaces) [29,30]. In particular, by employing a disjoining pressure term, modeling the liquid–solid micro-scale interactions, we avoided the implementation of any boundary condition at the contact line(s). With this approach, we examined cases of droplets impinging on complex solid surfaces, in good agreement with experimental measurements [29,30].

The aim of the current work is to extend our understanding regarding the driving mechanism and the dynamic behavior of a droplet on asymmetrically micro-structured substrates. In particular, we provide predictions regarding the migration velocity and the (dynamic) contact angle hysteresis under the effect of gravity or a periodic force induced by oscillating the bottom plate either in the horizontal or vertical direction. The effect of the solid structure length scale on the droplet motion is also investigated. Understanding the role of the structure asymmetry on the liquid transfer process has a great practical importance since it could enable the control of the droplet's speed and motion direction in modern miniaturized devices.

The present article is organized as follows: in Section 2, we describe the system of governing equations and outline the numerical scheme that is used for the simulations. Next, our numerical results regarding droplets moving on tilted as well as oscillated solid substrates are presented and discussed in Section 3. Concluding annotations are made in Section 4.

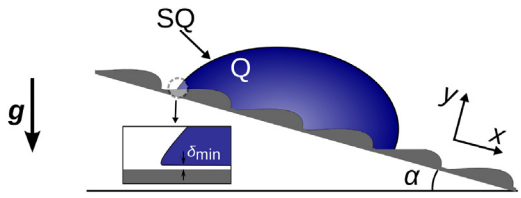


**Fig. 1.** Schematic of a droplet sliding on an asymmetrically structured substrate inclined at angle $a$ (notice that droplet and surface features are not shown in the same scale).

## 2. Mathematical formulation

We study the dynamics of a droplet sliding on a solid substrate which can be tilted by an inclination angle, $a$, or vibrated (horizontally or vertically). We consider that the droplet is a Newtonian incompressible fluid with nominal radius, $R_0$, density, $\rho$, viscosity, $\mu$ and surface tension, $\gamma$. Assuming that the viscosity of the ambient phase is negligible, the Navier–Stokes equations are solved only for the droplet interior (Q in Fig. 1). In our formulation the liquid–solid and liquid–vapor interfaces are treated uniformly, therefore the solution of the above set of equations is determined subject to a single stress balance boundary condition applied at the whole droplet surface (SQ in Fig. 1) referred as the liquid–ambient interface from now on [30]:

$$\boldsymbol{n}\cdot T_{\text{tot}} = (\boldsymbol{n}\cdot T_{\text{ext}}\cdot\boldsymbol{n})\boldsymbol{n} + (\boldsymbol{n}\cdot T_{\text{ext}}\cdot\boldsymbol{t})\boldsymbol{t} + 2\gamma\kappa\boldsymbol{n}. \tag{1}$$

In the above equation, $\boldsymbol{n}$, and, $\boldsymbol{t}$, are the unit normal and the unit tangent of the liquid–ambient interface, respectively; $T_{\text{tot}}$ and $T_{\text{ext}}$ are the total stress tensor and the stress tensor of the ambient phase, respectively, and, $\kappa$, is the mean curvature of the interface ($\kappa = -(\nabla_s\cdot\boldsymbol{n})/2$, where $\nabla_s$ is the surface gradient operator). In the above equation we have neglected any surface tension gradients that can be induced either by surfactant adsorption on the droplet surface [31,32] or by the presence of temperature gradients along the substrate [7], since such phenomena are out of the scope of this specific work.

Since the liquid–ambient interface is a closed curve, the droplet and the wall are always separated by an intermediate layer which is stabilized by the presence of normal micro-scale liquid–solid interactions [29,30]. The above is achieved by introducing a disjoining (Derjaguin) pressure term [33] which expresses the excess pressure on the interface due to the liquid–solid interactions. In this work the disjoining pressure is approximated by a Lennard–Jones type potential (alternative formulations could also be employed, see e.g. Kavousanakis et al. [34]):

$$p^{\text{LS}} = \frac{\gamma w^{\text{LS}}}{R_0}\left[\left(\frac{\sigma}{\delta/R_0+\epsilon}\right)^{C_1} - \left(\frac{\sigma}{\delta/R_0+\epsilon}\right)^{C_2}\right], \tag{2}$$

where, $\sigma$, and, $\epsilon$, are model parameters and, $\delta$, is the distance between solid and liquid phases (see also below). The parameters $C_1$ and $C_2$ regulate the cut-off distance (where, $p^{\text{LS}}\to 0$) of the liquid–solid interactions. The depth of the potential well is proportional to the wetting parameter, $w^{\text{LS}}$, which is directly related with the solid wettability (the Young contact angle, $\theta_Y$), as described in our previous work [29]. The disjoining pressure is finally introduced in the Navier–Stokes equations via the normal stress component of the interface force balance (Eq. (1)).

The distance of separation, $\delta$, between the liquid and the solid phases determines whether the disjoining pressure is attractive

(modeling van der Waals interactions, for relatively large $\delta$) or repulsive (modeling the overlapping of the electrical double layers, for small $\delta$). In the case of a perfectly flat solid surface, the distance, $\delta$, is defined as the vertical distance of the liquid surface from the solid boundary. When the solid surface is geometrically structured, the definition of distance, $\delta$, requires special consideration. Here, $\delta$, is obtained by solving the Eikonal equation [35], as proposed in our previous work [29]. The smallest allowable distance between the liquid and solid phases, $\delta_{\min}$ (see the inset of Fig. 1), where the repulsive and attractive micro-scale forces balance each other, can be approximately obtained for $p^{LS} = 0 \rightarrow \delta_{\min} = R_0(\sigma - \epsilon)$.

Regarding the tangential stress component of the interface force balance (Eq. (1)), we use a Navier slip model where the liquid–solid friction is regulated by an effective slip coefficient, $\beta_{\text{eff}}$ [30]. The effective slip coefficient (inverse slip length) is nonzero only close to the solid surface, thus a partial slip boundary condition is implemented along the liquid–solid interface whereas a shear-free boundary condition is applied on the liquid–vapor interface [30].

In order to account for the deforming physical domain due to the droplet deformation we combine the above equations with an elliptic mesh generation scheme and the position of the liquid–ambient interface is tracked using the kinematic boundary condition, as presented in our previous work [29,30].

Finally, to reduce the overall computational cost, we assume translational symmetry along a direction perpendicular to the $xy$-plane (see Fig. 1), which renders the present model two-dimensional. The final set of equations is discretized using the finite element method (FEM) [36] while integration in time is performed using the implicit Euler method; the code has been implemented in COMSOL Multiphysics® commercial software. A sensitivity analysis regarding the size of computational mesh can also be found in the Supplementary Material.

## 3. Results

We begin our study by examining the flow dynamics of a glycerin/water mixture droplet (85% of glycerin, $\rho = 1275\,\text{kg/m}^3$, $R_0 = 1.5\,\text{mm}$, $\gamma = 0.07\,\text{N/m}$ and $\mu = 116\,\text{mPa s}$) sliding on inclined surfaces with different topographies (both symmetrically and asymmetrically structured). Then we study the effect of solid vibration on the movement of droplets on asymmetrically structured surfaces. We have selected the glycerin/water mixture droplets (instead of water droplets) so as to minimize the inertial effects and highlight the role of the solid surface asymmetric structure. Considering that the disjoining pressure parameters do not significantly affect the obtained results (see the sensitivity analysis presented in the Supplementary Material), we selected their values in accordance with our previous work [29,30], namely: $C_1 = 12$, $C_2 = 10$, $\sigma = 9 \times 10^{-3}$ and $\epsilon = 8 \times 10^{-3}$. Furthermore, in order to recover the no-slip boundary condition along the solid surface, we consider a large value of the effective slip coefficient. The flow dynamics remain practically unaffected beyond this large value, as demonstrated in our previous work [30]. The variety of problems which are examined in the present paper (involving sliding, and vibrated droplets) renders the definition of particular characteristic quantities complicated and thus we prefer to present the results of our simulations in dimensional form. This is by no means restrictive since dimensionless groups are introduced where deemed necessary to draw conclusions on the importance of different physical mechanisms.

### 3.1. Droplet sliding on inclined structured surfaces

In a recent work [30] we have examined the mobility of a droplet on two kinds of textured substrates, favoring either the Wenzel (the droplet fully penetrates the micro-structure [37]) or the Cassie (air pockets are trapped in the micro-structure [37]) wetting state. In particular, as observed in Fig. 2, we considered:

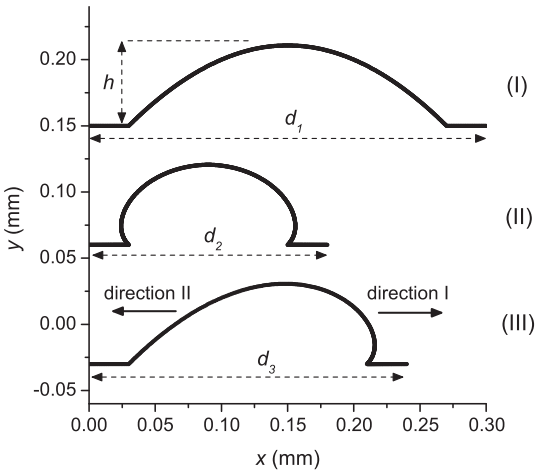


**Fig. 2.** Unit structure of the different substrate cases. The elementary corrugation of the asymmetric surface (III) is a combination of the basic structure of the two symmetric surfaces (I, II).

a) A symmetrically structured striped surface (symmetric surface I) featuring smooth protrusions of width $d_1 = 0.3$ mm that favors the Wenzel wetting state and
b) A symmetrically structured striped surface (symmetric surface II) with mushroom like cross-sectional shape that promotes the Cassie wetting state. In this case the width of the stripes, $d_2$, is 0.18 mm

We have found that the presence of air pockets trapped in the solid structure (Cassie wetting state) leads to an increased mobility of the droplet as it slides on an inclined substrate. The above argument was also in qualitative agreement with experimental observations [38]. The aim here is to study the droplet dynamic behavior on an asymmetrically structured surface. The asymmetric surface is formed by merging the halves of each symmetric unit structure studied in our previous work. Then a hybrid structure of width $d_3 = 0.24$ mm arises (III in Fig. 2). The height of the protrusions is identical for the three structures, $h = 0.06$ mm; note that the ratio of the height, $h$, over the initial droplet diameter, $2R_0$, is 1/50. We also consider that the solid material is hydrophobic ($\theta_Y = 130^\circ$).

Initially, we observe that for $\alpha = 0^\circ$ (the substrate is not inclined) the droplet rests on a Cassie state on the asymmetric surface, where however the liquid meniscus is sloping between the protrusions (see Fig. 3). Furthermore, in order to investigate the dynamic behavior of the droplet in different directions, we tilt the left end of the

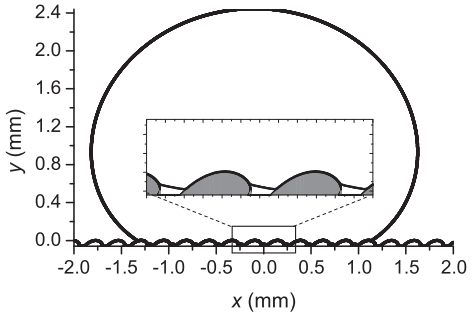


**Fig. 3.** Equilibrium profile of a droplet on an asymmetrically patterned surface with $\theta_Y = 130^\circ$.

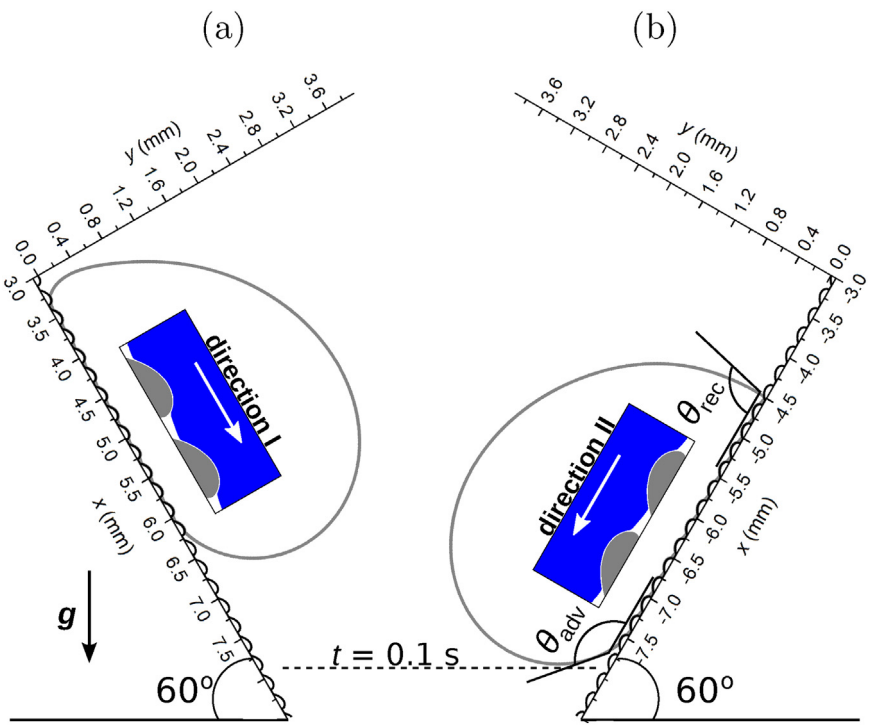


**Fig. 4.** Profiles (at $t = 0.1$ s) of a glycerin/water mixture droplet, sliding on two different directions (a: forward and b: against the corrugations tilt) of an asymmetrically structured inclined substrate.

asymmetric substrate either upwards or downwards, as presented in Fig. 4. In the first case ($a = 60^\circ$) the droplet moves to the right (toward the direction of the corrugations tilt), defined as direction I, whereas in the latter case ($a = -60^\circ$) the droplet moves to the left (opposite to the direction of the corrugations tilt), which is defined as direction II (see also Fig. 2). Interestingly, it is observed that the droplet exhibits different migration velocities, according to the direction of motion on the asymmetrically structured substrate. In particular, as shown in Fig. 4, for the same period of time ($t = 0.1$ s) the droplet has covered larger distance when moving in the direction II.

By comparing, in Fig. 5, the droplet migration velocity on the different solid substrate cases (symmetric surface I, II and asymmetric surface) we notice an acceleration phase (sharp increase of the velocity) at early times (for $t < 0.02$ s) whereas for later times ($t > 0.07$ s) the migration velocity reaches a plateau value. The observed fluctuations of the velocity around the plateau value can be attributed to the contact line pinning and de-pinning on the substrate corrugations. In more detail, we observe that the asymmetric surface behaves in a similar fashion with the symmetric surface I (exhibiting stronger adhesion) when the droplet advances in the direction I, whereas the dynamics compare to the ones of the symmetric surface II (facilitating the droplet sliding) when the fluid moves in the direction II.

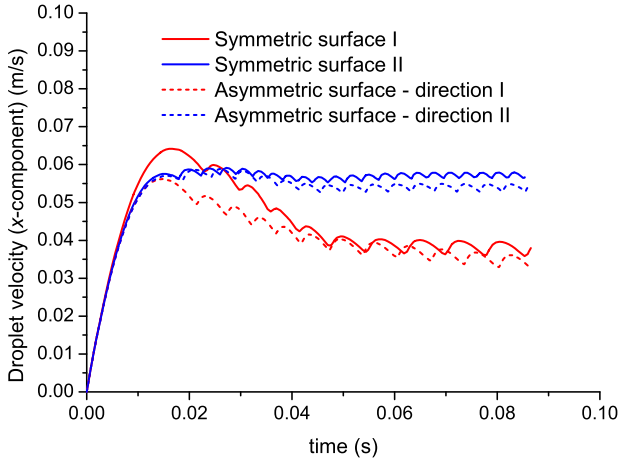


**Fig. 5.** Temporal evolution of the average $x$-component of the velocity for a glycerin/water mixture droplet on different kinds of solid surfaces. The two different motion directions for the asymmetric solid surface are presented with dashed lines of different color (red – direction I, blue – direction II). The absolute value of the velocity is used in the case where the droplet is moving in the negative direction II). (For interpretation of the references to color in this figure legend, the reader is referred to the web version of this article.)

### 3.1.1. *Preferable motion direction*

In our previous work [30], we have attributed the difference in the migration velocity, between the two symmetrically structured surfaces, to the presence of trapped air pockets in the Cassie state. However, in the case of asymmetric texturing the droplet is always in the Cassie state no matter whether it moves in the direction I or II (see Fig. 4) and therefore the contact area between liquid and solid remains roughly the same. Thus the preference in the motion direction has to arise due to the local forces applied in the contact line region. A study regarding the capillary retention forces developed at the contact line of a droplet on asymmetric features has been performed by Extrand [39]. In particular, it is calculated that the force resisting the droplet motion, originated by the interfacial tension acting at the contact line of a sessile droplet, is defined as:

$$F_i = kR_0\gamma(\cos\theta_{rec} - \cos\theta_{adv}), \quad (3)$$

where $k$ is a prefactor which depends on the shape of the contact line, $\theta_{adv}$ and $\theta_{rec}$ are the macroscopically observed advancing and receding contact angles of the droplet, respectively (see Fig. 4). In our simulation the capillary forces are predominant against the viscous forces (the capillary number is below unity, $Ca = \mu u^*/\gamma = 0.2$, where, $u^* = \sqrt{\|\boldsymbol{g}\|R_0}$, is a characteristic velocity with, $\boldsymbol{g}$, the gravitational acceleration) therefore the capillary net force that resists the droplet motion on the different directions

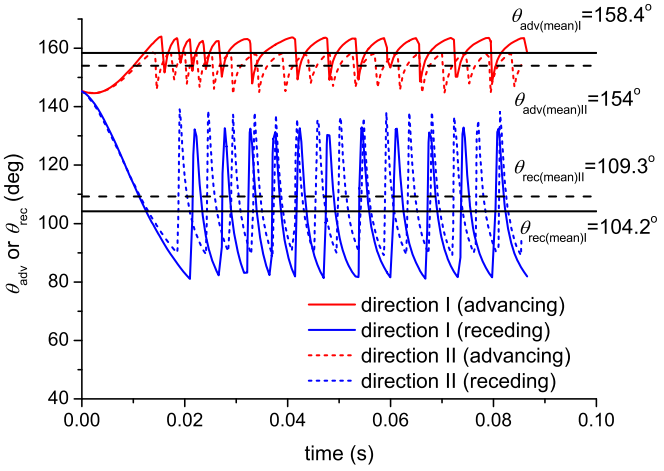


**Fig. 6.** Advancing and receding contact angles of a glycerin/water mixture droplet sliding on an inclined ($a = 60^\circ$) asymmetrically structured surface. The solid lines correspond the direction coinciding the corrugations tilt (I) whereas the dashed lines correspond to the opposite direction of motion (II). The mean value for each advancing and receding contact angles is also presented.

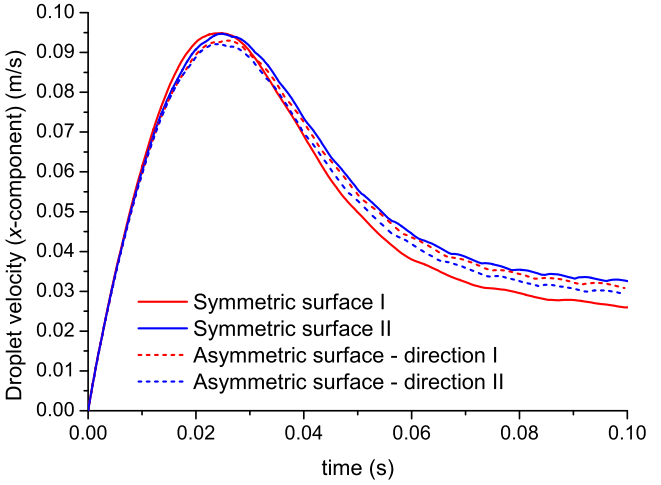


**Fig. 8.** Temporal evolution of the average $x$-component of the velocity for a surfactant-bearing glycerin/water mixture droplet on different kinds of solid surfaces.

should be critical. Furthermore, the advancing and receding contact angles can be easily predicted by our proposed scheme as shown in Fig. 6. In particular, the slope of the droplet surface is evaluated, against the inclined plane, at a fixed distance ($y = 1 \times 10^{-2} R_0$) from the substrate, where the action of the disjoining pressure has been effectively vanished. Despite the fact that the dynamic contact angles exhibit fluctuations (due to the contact line pinning–depinning on the substrate corrugations [30]) our results show that the mean contact angle hysteresis, $\Delta\theta$ (the difference between the advancing and the receding contact angles) is smaller when the droplet slides in the slippery direction (II). In particular $\Delta\theta_{\mathrm{I}} = \theta_{\mathrm{adv(mean)I}} - \theta_{\mathrm{rec(mean)I}} = 158.4^\circ - 104.2^\circ = 54.2^\circ$, whereas $\Delta\theta_{\mathrm{II}} = \theta_{\mathrm{adv(mean)II}} - \theta_{\mathrm{rec(mean)II}} = 154^\circ - 109.3^\circ = 44.7^\circ$. Therefore, the retention capillary force in direction I, $F_{\mathrm{I}}$, significantly exceeds the one in the opposite direction, $F_{\mathrm{II}}$, and their ratio is $F_{\mathrm{I}}/F_{\mathrm{II}} = 1.23$ (the values of $F_{\mathrm{I}}$, $F_{\mathrm{II}}$ are calculated by using Eq. (3)). We note that the preferred motion direction predicted here is in line with the theoretical work of Extrand [39], as well as the experimental works of Buguin et al. [15] who studied droplets moving on vibrated asymmetrically structured substrates, and Contraires et al. [40] who considered droplets growing asymmetrically on asymmetric asperities.

A critical question is whether a change in the capillary forces magnitude (e.g. by using a surfactant to lower the surface tension) could affect the preferable motion direction of the droplet. In particular, in Fig. 7 we compare the profiles of a surfactant-bearing (gray line) and a normal glycerin/water mixture droplet when sliding at the same direction (II) of the asymmetrically structured surface, at $t = 8.5 \times 10^{-2}$ s. Despite the fact that the surface tension has been significantly reduced ($\gamma = 0.014$ N/m, which corresponds to a capillary number, $\mathrm{Ca} \approx 1$), we notice that the liquid is still suspended above the protrusions (Cassie state) for the surfactant-bearing case (see the inset of Fig. 7). Aiming to examine the dynamic behavior of the surfactant-bearing droplet on all the previously studied substrates, we plot in Fig. 8 the temporal evolution of the average $x$-component of the velocity. Interestingly enough, we observe that the droplet behaves similarly for all the substrate cases. In particular, any differences in the droplet migration velocity, when moving on different symmetrically structured substrates, as well as on different directions on the asymmetrically patterned substrate, are negligible. The above argument cannot be attributed, in the latter case, to the change of the wetting state (i.e. from Cassie to Wenzel state) since the liquid on the asymmetrically patterned surface is suspended above the protrusions in both cases (with and without surfactant). Such a conclusion is important for selecting suitable liquids in cases where a directional droplet motion is required. In particular, a low surface tension liquid seems to be inappropriate.

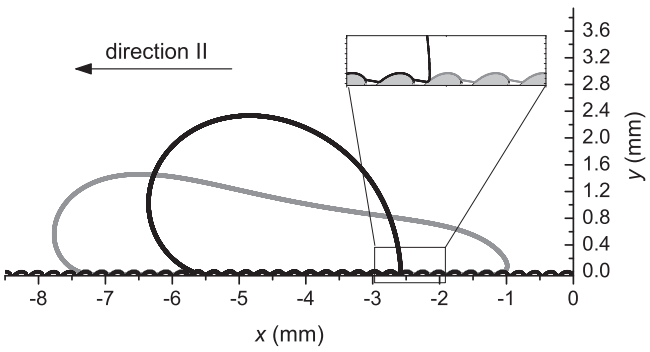


**Fig. 7.** Snapshots of a surfactant-bearing (gray line) versus a normal (black line) glycerin/water mixture droplet, sliding ($a = -60^\circ$) in the direction II of the asymmetric surface, at $t = 8.5 \times 10^{-2}$ s.

### 3.2. Droplet on a vibrated asymmetrically structured surface

Despite the fact that transferring droplets on tilted substrates has a practical importance in some applications (e.g. fog harvesting [41]), the active control of the droplet migration velocity (e.g. in lab-on-a-chip devices) requires an external stimuli. Such an actuation can be achieved by applying horizontal or vertical forced oscillations on the solid substrate.

#### 3.2.1. Effect of the vibration frequency

The effect of several parameters (frequency, direction, amplitude of the oscillation, length scale of the solid texture) on the droplet motion is investigated in this Section. We initially consider a droplet on an asymmetrically structured substrate subjected to a forced sinusoidal vibration either at the vertical or horizontal direction. The position of the solid substrate for each of the two cases is described by the following equations:

$$y = y_0 - A\sin(\omega t), \tag{4a}$$

$$x = x_0 - A\sin(\omega t), \tag{4b}$$

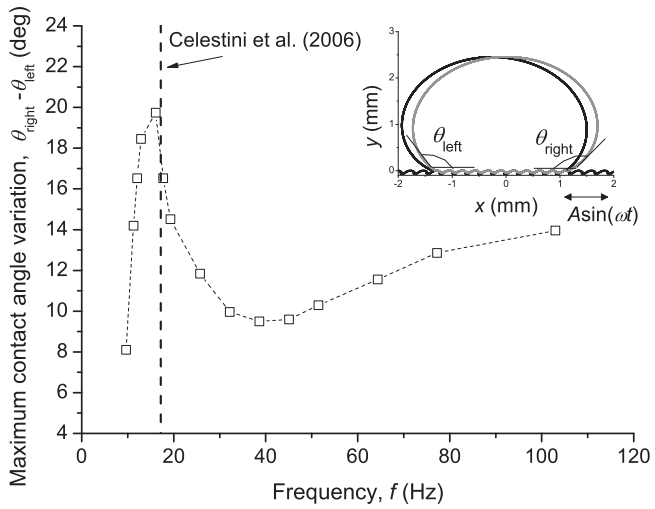


**Fig. 9.** Maximum contact angle variation as a function of the frequency of the horizontal vibration. The semianalytical prediction of Celestini et al. [44] for the resonance frequency is presented with the dashed line (see Eq. (5)).

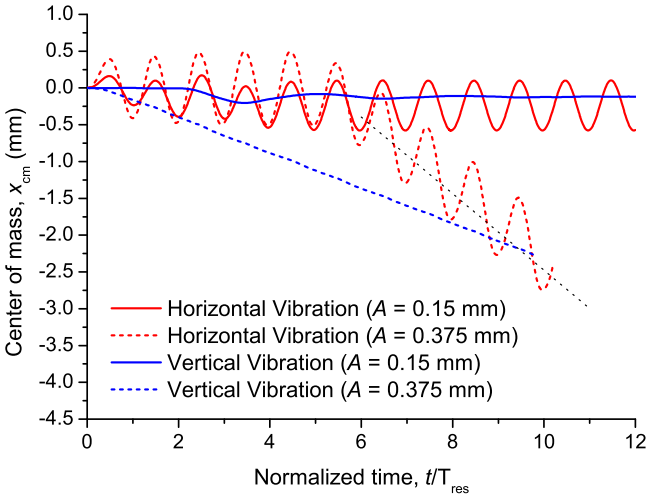


**Fig. 11.** Temporal evolution of the droplet's center of mass (the horizontal position), $x_{cm}$, for different vibration directions (horizontal and vertical) and magnitudes, $A$. The normalized time is defined as $t/T_{res}$ where $T_{res}$ is the oscillation period which corresponds to the resonance ($T_{res} = 1/f_{res}$). An average value of the droplet's center of mass, for $A = 0.375$ mm in the case of horizontal vibrations, is presented by the black dotted line.

where $x_0$, $y_0$ are the positions at $t = 0$; $A$ is the oscillation amplitude and, $\omega$, denotes the angular frequency. In order to maximize the effect of vibration on the droplet motion and to minimize the energy damping, it is reasonable to set the frequency, $f = \omega/2\pi$, to the resonance frequency of the system [42]. It is well known that the resonance frequency strongly depends on the droplet size and the liquid properties [43]. Moreover, in the case of a supported droplet on a structured substrate the resonance frequency depends on the detailed equilibrium droplet shape on the corrugated surface (it has been demonstrated that several equilibrium droplet shapes can be accommodated on a certain structured substrate [34]). The above requires detailed computations of the droplet shape and dynamic behavior on such a complex surface.

Here, we detect the resonance by computing the dependence of the deformation of the droplet on the applied frequency. A simple measure of the deformation for the horizontal oscillations is the maximum difference between the right and the left contact angles (see Fig. 9); for vertical oscillations we select the aspect ratio of the droplet profile (see Fig. 10). Therefore, by using a small oscillation amplitude ($A = 0.075$ mm) we calculate that the maximum deformation appears at $f_{res,h} = 16.1$ Hz for the horizontal and $f_{res,v} = 45.05$ Hz for the vertical vibrations. At this point, it would be interesting to test our predictions against the existing theoretical models.

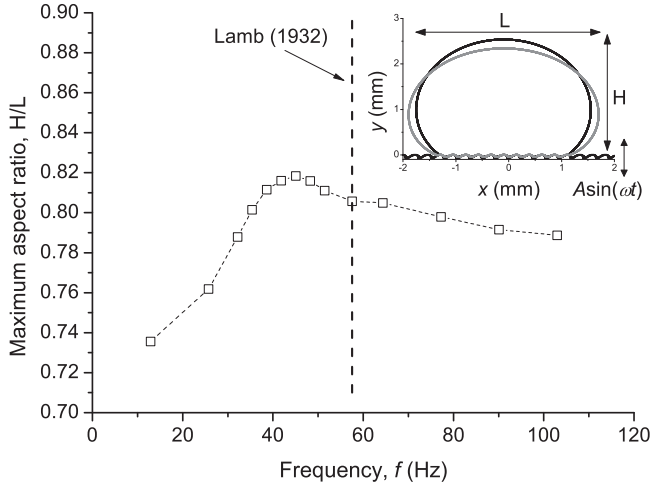


**Fig. 10.** Maximum aspect ratio of the droplet profile as a function of the frequency of the vertical vibration. An analytical prediction for the resonance frequency, proposed by Lamb [45], is depicted with the dashed line (see Eq. (6)).

For predicting the resonance frequency of horizontally vibrated droplets Celestini et al. [44] proposed a semianalytical expression. In particular, by using a simple oscillator analogy they concluded that the resonance angular frequency of a two-dimensional droplet under the influence of horizontal vibrations is estimated by:

$$\omega_0 = \sqrt{\frac{6\gamma H(\theta_Y)}{\rho(1-\cos\theta_Y)(2+\cos\theta_Y)}} R_0^{-3/2}, \quad (5)$$

where the function $H(\theta_Y)$, which is computed by static simulations, incorporates the effect of droplet deformation [44]. The agreement between our simulation and the prediction of Celestini et al. (see Fig. 9) corroborates to the reliability and accuracy of our scheme. Unfortunately, there is no such formula for the vertical vibrations case, however, our results can be roughly compared with a general expression, proposed by Lamb [45], for the $n$th vibration mode of a three-dimensional free liquid droplet:

$$\omega_n = \sqrt{\frac{n(n-1)(n+2)\gamma}{\rho {R_0}^3}}. \quad (6)$$

The fundamental frequency ($n = 2$) predicted by Eq. (6) deviates from our computations (see Fig. 10) due to the contribution of the contact line pinning effects that were obviously not taken into account in the theoretical work of Lamb [45].

### 3.2.2. *Effect of the vibration direction*

We have already shown that the asymmetric structure may set a preferential direction of motion in the case of gravity-driven droplet migration. A question that may arise is whether it is possible to exploit the asymmetric features in order to set a droplet to motion by applying either vertical or horizontal vibrations. In Fig. 11 we present the temporal evolution of the droplet's center of mass (the horizontal position), $x_{cm}$, as a function of oscillation direction and amplitude. The forced frequency for each case corresponds to the resonance ($f_{res}$), as calculated in the previous Section for a glycerin/water mixture droplet. Note that in order to depict both cases of horizontal and vertical vibrations in a single graph, and given that the oscillation frequency differ (16.1 Hz

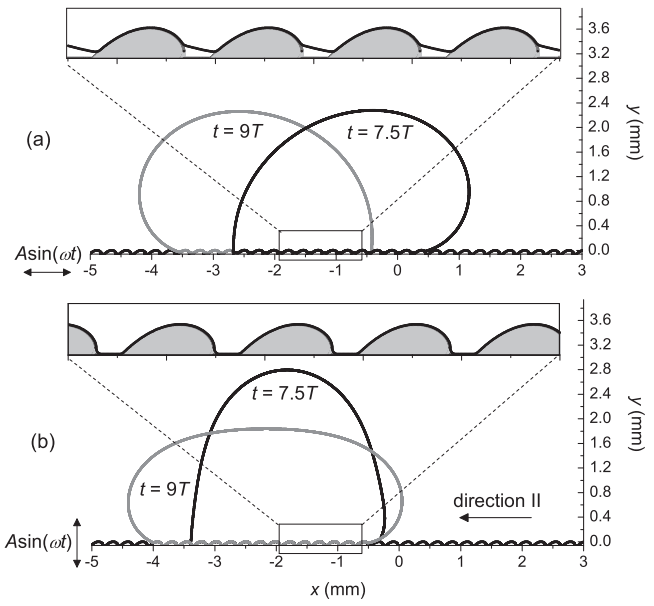


**Fig. 12.** Snapshots of a glycerin/water mixture droplet moving on an asymmetrically structured solid surface which is vibrated (a) horizontally and (b) vertically on the resonance frequency for each case. A magnification of the droplet profiles, close to the solid surface, is presented in the insets. Video clips of the moving droplets on the vibrated substrates can be found in the Supplementary Material.

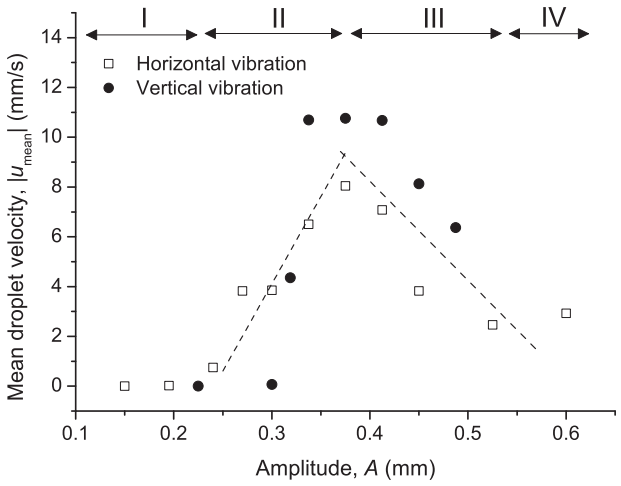


**Fig. 13.** Absolute value of the average droplet migration velocity during two oscillation periods (from 6$T$ to 8$T$), as a function of the amplitude, $A$, for horizontal and vertical vibrations. The oscillation frequency corresponds to the resonance for each case. Dashed lines (linear fit to the computational data) are drawn as guide to the eye. Video clips of the moving droplets on the vibrated substrates are included in the Supplementary Material (for $A = 0.375$ mm).

for the horizontal and 45.05 Hz for the vertical vibrations, respectively), time is expressed here in dimensionless units. It is observed that for a small oscillation amplitude ($A = 0.15$ mm) the droplet deforms but does not move along the substrate (see Fig. 11). However, for a vibration amplitude larger than the width of the solid protrusions ($A = 0.375$ mm $> d_3 = 0.24$ mm) the liquid moves to the direction opposing the corrugations tilt (direction II). The motion direction here conforms to the preferable sliding direction in the case where the asymmetrically structured solid surface is tilted (see previous Section).

Despite the fact that the liquid moves to the same direction for both horizontal and vertical substrate oscillations, the dynamic behavior of the droplet significantly differs. In particular, as observed in Fig. 11, the droplet motion is smoother in the case of vertical oscillations whereas it exhibits strong fluctuations when the substrate is vibrated horizontally. Moreover, in contrast with the vertical oscillation case where the droplet starts to migrate almost immediately, the droplet starts to move after a time of ∼5 periods (5$T$) in the case of horizontal vibrations. Interesting observations can also be made by zooming at the droplet shape near the solid surface. In particular, in Fig. 12 we present different snapshots of the droplet (for $t = 7.5T$ and 9$T$, where $T = T_{res}$ for each case) by applying horizontal and vertical forced vibrations ($A = 0.375$ mm). Note that in both time instances ($t = 7.5T$ and 9$T$) the solid substrate is at the same position although the acceleration direction is opposite. It is observed that in the case of horizontal oscillations the droplet sits on top of the protrusions, minimizing the contact area between the liquid and the solid phases (Cassie state). On the other hand, the picture is different for the vertical oscillations where the liquid fully penetrates the solid asperities (Wenzel state). In particular, the higher momentum developed in the $y$-direction facilitates the collapse from Cassie to Wenzel wetting state. The migration velocity is expected to be lower in this case since it is known that Wenzel wetting states exhibit high friction and thus low droplet mobility [38]. Such a behavior can be actually observed in Fig. 11, where the droplet migrates faster in the case of horizontal vibration (black dotted line). The different rate in the energy dissipation may also be responsible for this discrepancy (the droplet deforms to a greater extend in the case of vertical vibrations). A detailed analysis regarding the energy dissipation rate will be presented in the following Section.

### 3.2.3. *Effect of the vibration amplitude*

We have shown that a droplet migrates uni-directionally on an asymmetrically structured surface when the oscillation amplitude is larger than a threshold value, however it is important to understand better the factors that affect the droplet migration velocity. Next, we perform a throughout investigation of the droplet dynamic behavior as a function of the vibration amplitude.

In Fig. 13 we depict the mean value of the droplet migration velocity (computed between two oscillation periods) for different amplitudes. In particular the mean velocity is estimated by $u_{mean} = \delta x_{mean}/(8T - 6T)$, where $\delta x_{mean}$ is the change of the droplet's center of mass (horizontal position) between the 6th and the 8th oscillation periods.

As observed in Fig. 13, the mean droplet velocity is very sensitive to the vibration amplitude. In particular, we observe four different regimes:

(I) For low vibration amplitudes ($A < 0.2$ mm) the external force is not enough to surpass the static hysteresis and thus no motion is detected.
(II) Exceeding a vibration amplitude threshold ($A = 0.24$ mm for the horizontal and 0.32 mm for vertical oscillations, respectively) the friction in direction II is surpassed and the droplet migrates with a mean velocity, $u_{mean}$. The latter is observed to increase linearly with the amplitude.
(III) As the amplitude further increases, the vibration gets so intense that the contact angle hysteresis can be surpassed in both directions. The above results to a decrease in the average droplet velocity. The critical amplitude, $A_{crit}$, where the migration velocity is maximal equals to 0.375 mm for the horizontal vibration case whereas is ranges from 0.34 mm to 0.41 mm for the vertical oscillations. A similar behavior, where the migration velocity is reduced for large vibration amplitudes, has also been reported experimentally [15] which strengthens the validity of our simulations.

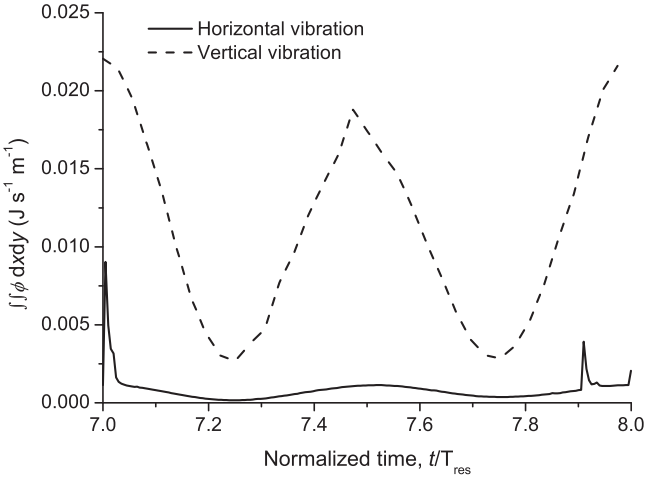


**Fig. 14.** Surface integral of the energy dissipation function, $\phi$, during an oscillation cycle (from $t = 7T$ to $t = 8T$), for both horizontal and vertical vibration cases.

(IV) Finally, the mean velocity is stabilized for larger vibration amplitudes.

Considering that during an oscillation period, $T$, the droplet moves along a number of solid unit cells, $n_s$, the average velocity equals to: $u_{mean} = n_s d_3/T$, where $d_3$ is the width of the unit cell structure of the asymmetric substrate (see Fig. 2). Consequently, when the migration velocity is maximal (8 mm/s for the horizontal and 10.8 mm/s for the vertical vibration) the droplet is shifted by two solid structure corrugations for the horizontal and one for the vertical oscillations. Given that the lateral displacement of the droplet by one corrugation requires overcoming an energy barrier [46] (constant for both vibration cases), we would expect that the peak potential energy of the droplet is larger in the case of the horizontal vibration. This is not the case though: by evaluating the peak potential energy, $E_{tot}$, per unit mass, $M$, at $A = A_{crit}$ and $f = f_{res}$:

$$\frac{E_{tot}}{M} = \pi f_{res}^2 A_{crit}^2, \tag{7}$$

we conclude that the peak energy of the vertical is considerable higher compared with the horizontal vibrations, $E_{tot,ver}/E_{tot,hor} = 7.83$ (we considered an average value of $A_{crit} = 0.375$ mm for the vertical vibration case). The lateral displacement per cycle, however, is smaller in the first case. An explanation for this behavior can be derived by examining the energy dissipation for both vibration cases.

In Fig. 14 we present the surface integral, over the entire cross-sectional droplet area, $A_{droplet}$, of the dissipation function, $\phi$, which reads in Cartesian coordinates [47]:

$$\phi = T_{tot} : \nabla \boldsymbol{u} = 2\mu \left[ \left( \frac{\partial u_x}{\partial x} \right)^2 + \left( \frac{\partial u_y}{\partial y} \right)^2 \right] + \mu \left[ \left( \frac{\partial u_x}{\partial y} \right) + \left( \frac{\partial u_y}{\partial x} \right) \right]^2, \tag{8}$$

where $\boldsymbol{u}$ is the fluid velocity field. It is clear from our results that the rate of dissipation is substantially larger in the case of vertical vibrations. This is also evident by looking at the droplet deformation for the two cases (see Fig. 12). In particular, the total energy, per droplet depth, consumed during a cycle is: $E_{diss,hor} = \int_{7T}^{8T} \iint_{A_{droplet}} \phi \mathrm{d}x\mathrm{d}y\mathrm{d}t =$ $5.05 \times 10^{-5}$ J/m and $E_{diss,ver} = 2.34 \times 10^{-4}$ J/m for the horizontal and vertical oscillations, respectively.

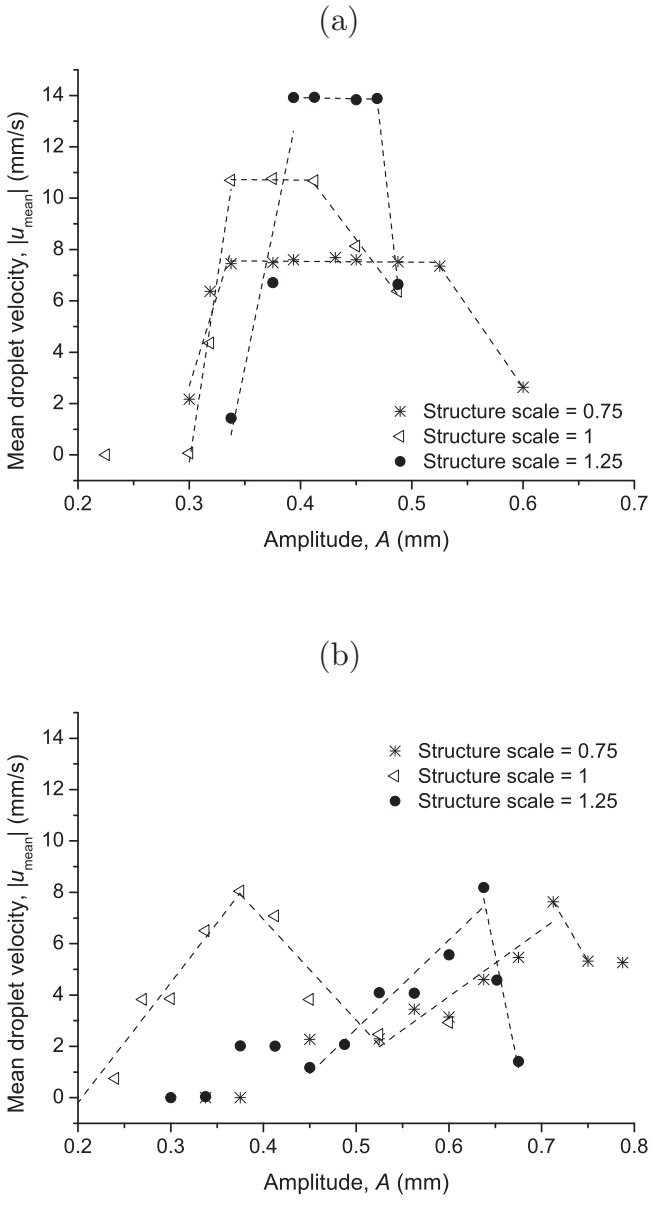


**Fig. 15.** Absolute value of the average droplet migration velocity on substrates with different structure scalings subjected to (a) vertical and (b) horizontal vibrations. The oscillation frequency corresponds to the resonance for each case. Dashed lines (linear fit to the computational data) are drawn as guide to the eye.

### 3.2.4. *Effect of the structure length scale*

Useful conclusions can be derived by proportionally modifying the size of the solid structure unit cell. In particular, in Fig. 15 we present the dependence of the mean droplet velocity on the texture scaling, $s$. In the studied cases, the width the asymmetric unit structure ranges from 0.18 mm ($s = 0.75$) to 0.3 mm ($s = 1.25$) and the height from 0.045 mm to 0.075 mm, respectively. The frequency of each vibration is set to the corresponding resonance, which is evaluated as described above for each case.

Starting from the vertical forced vibrations (Fig. 15a) we observe a plateau value of the velocity within a range of amplitudes. The above range decreases by increasing the structure scaling while at the same time the migration velocity increases. On the other hand, there is a sharp maximum (for $A = A_{crit}$) of the migration velocity in the case of horizontal vibrations (Fig. 15b). Specifically, we observe the critical value of the amplitude is a non-linear function of the structure scaling (i.e. $A_{crit}$ decreases from 0.725 mm to 0.375 mm

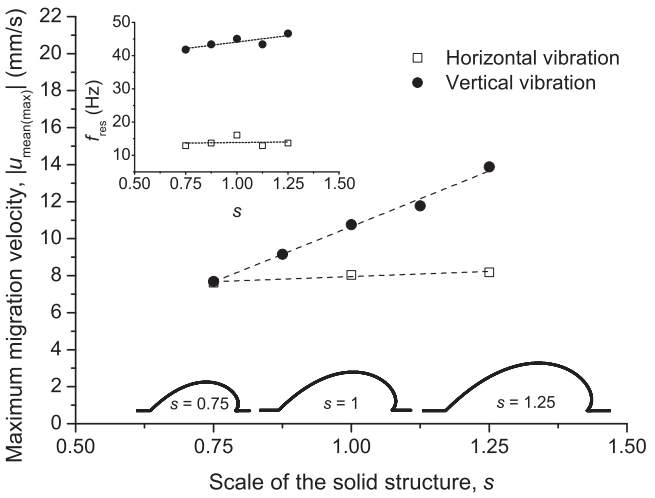


**Fig. 16.** Maximum migration velocity as a function of the solid structure scale, for both horizontal and vertical oscillations. The case where $s = 1$ corresponds to the initial unit structure presented in Fig. 2. The oscillation frequency and amplitude correspond to $f_{res}$ and $A_{crit}$, respectively, for each case. The dependence of the resonance frequency on the structure scaling is presented in the inset.

as the texture scale grows from 0.75 to 1 and then increases again to 0.65 mm for the larger structure scale, $s = 1.25$). This behavior can be attributed to the fact that the anisotropic wetting properties gradually fade when reducing the structure scaling, thus requiring larger oscillation amplitude to start the droplet motion. The latter depends on the maximum difference between the right and the left contact angles (see Eq. (3)) which is observed to reduce, for a static droplet, as the structure size is shrinked (from $\Delta\theta = 2^\circ$, at $s = 1.25$ to $\Delta\theta = 0.2^\circ$, at $s = 0.75$). In addition, large amplitude is also required when the structure scale is magnified, since the droplet needs to be deformed to a greater extend in order to migrate. Therefore, fine tuning the amplitude of the horizontal oscillations, for an effective droplet migration in experimental practice, seems to be a tedious task, unless a predictive model for the droplet behavior, as the one described here, is employed.

An overall picture can be obtained by plotting in Fig. 16 the maximum migration velocity of the droplet, $|u_{mean(max)}|$, as a function of the solid structure scale, $s$. Interestingly enough, it is observed that the migration velocity increases linearly with the texture scaling for the vertical vibration case. The above behavior is attributed on one hand to the larger distance covered by the droplet during a cycle (since the space between the protrusions is increased), and on the other hand to the amplified effect of the unbalanced capillary retention force at the contact line. Furthermore, in the case of horizontal vibrations the migration velocity is not affected by changing the structure scaling. Such a behavior signifies a reduced influence of the solid structure on the droplet velocity in this case which may be attributed to the limited droplet deformation, in contrast with the vertical vibrations (see also Fig. 12). The same analysis is performed for the resonance frequency (see the inset of Fig. 16) which also seems to change slightly with the length scale of the solid structure.

## 4. Conclusions

It has been demonstrated that an asymmetrically structured surface can successfully reproduce two kinds of wetting behaviors: (a) a slippery behavior (resembling the Cassie regime), when the substrate is tilted downward (against the corrugations tilt, for $a < 0^\circ$) and (b) a sticky behavior (resembling the Wenzel regime), when the substrate is tilted upward (forward the corrugations tilt, for $a > 0^\circ$). Our simulations indicate that this behavior can be attributed to the unbalanced capillary retention force at the contact line. Thus, in cases where the capillary effect is weakened (e.g. for a surfactant-bearing droplet) we observed that the anisotropic friction behavior fades.

We have also examined cases where the droplet displacement is induced by a forced vibration of the solid substrate. Once again the droplet follows the direction prescribed by the capillary forces (opposing the corrugations tilt), after a threshold value of the oscillation amplitude has been surpassed. Moreover, we have found that the migration velocity is maximal for a certain oscillation frequency and amplitude values (at $f = f_{res}$ and $A = A_{crit}$). Finally, we have demonstrated a link between the droplet migration velocity and the length scale of the solid structure. In particular, when applying vertical vibrations, the migration velocity is appeared to be a linear function of the texture scaling. This is not the case, however, when the droplet is set to motion by horizontal vibrations. In the latter situation the migration velocity is not seriously affected by the structure length scale.

Future work focuses on further investigation of the geometric characteristics effect on the droplet motion. In particular, our main goal is to efficiently evaluate the energy barriers for droplet motion outset in the two directions (opposing and coinciding the corrugations tilt). By using such a tool, accompanied with dynamic simulations, we could design more effective asymmetric structures that promote the uni-directional motion of a droplet under varying external conditions.

## Acknowledgements

The authors kindly acknowledge funding from the European Research Council under the Europeans Community's Seventh Framework Programme (FP7/2007–2013)/ERC grant agreement no. [240710]. We are also grateful to Dr. George Pashos (National Technical University of Athens) for the useful discussions on the subject.

## Appendix A. Supplementary data

Supplementary data associated with this article can be found, in the online version, at http://dx.doi.org/10.1016/j.colsurfa.2016.09.078.

## References

[1] J. Bico, U. Thiele, D. Quéré, Wetting of textured surfaces, Colloids Surf. A: Physicochem. Eng. Aspects 206 (1) (2002) 41–46.
[2] X. Feng, L. Jiang, Design and creation of superwetting/antiwetting surfaces, Adv. Mater. 18 (23) (2006) 3063–3078.
[3] N.J. Shirtcliffe, G. McHale, S. Atherton, M.I. Newton, An introduction to superhydrophobicity, Adv. Colloid Interface Sci. 161 (1) (2010) 124–138.
[4] Y. Temiz, R.D. Lovchik, G.V. Kaigala, E. Delamarche, Lab-on-a-chip devices: how to close and plug the lab? Microelectron. Eng. 132 (2015) 156–175.
[5] E. Gauthier, T. Hellstern, I.G. Kevrekidis, J. Benziger, Drop detachment and motion on fuel cell electrode materials, ACS Appl. Mater. Interfaces 4 (2) (2012) 761–771.
[6] F. Lapierre, M. Jonsson-Niedziolka, Y. Coffinier, R. Boukherroub, V. Thomy, Droplet transport by electrowetting: lets get rough!, Microfluid. Nanofluid. 15 (3) (2013) 327–336.
[7] G. Karapetsas, K.C. Sahu, K. Sefiane, O.K. Matar, Thermocapillary-driven motion of a sessile drop: effect of non-monotonic dependence of surface tension on temperature, Langmuir 30 (15) (2014) 4310–4321.
[8] G. Lagubeau, M. Le Merrer, C. Clanet, D. Quéré, Leidenfrost on a ratchet, Nat. Phys. 7 (5) (2011) 395–398.
[9] A. Wixforth, C. Strobl, C. Gauer, A. Toegl, J. Scriba, Z. Guttenberg, Acoustic manipulation of small droplets, Anal. Bioanal. Chem. 379 (7) (2004) 982–991, http://dx.doi.org/10.1007/s00216-004-2693-z.
[10] P. Brunet, J. Eggers, R. Deegan, Vibration-induced climbing of drops, Phys. Rev. Lett. 99 (14) (2007) 144501.
[11] X. Noblin, R. Kofman, F. Celestini, Ratchetlike motion of a shaken drop, Phys. Rev. Lett. 102 (19) (2009) 194504.

[12] K. John, U. Thiele, Self-ratcheting stokes drops driven by oblique vibrations, Phys. Rev. Lett. 104 (10) (2010) 107801.
[13] R. Borcia, I.D. Borcia, M. Bestehorn, Can vibrations control drop motion? Langmuir 30 (47) (2014) 14113–14117.
[14] O. Sandre, L. Gorre-Talini, A. Ajdari, J. Prost, P. Silberzan, Moving droplets on asymmetrically structured surfaces, Phys. Rev. E 60 (3) (1999) 2964.
[15] A. Buguin, L. Talini, P. Silberzan, Ratchet-like topological structures for the control of microdrops, Appl. Phys. A 75 (2) (2002) 207–212.
[16] T.A. Duncombe, E.Y. Erdem, A. Shastry, R. Baskaran, K.F. Böhringer, Controlling liquid drops with texture ratchets, Adv. Mater. 24 (12) (2012) 1545–1550.
[17] N. Tretyakov, M. Müller, Directed transport of polymer drops on vibrating superhydrophobic substrates: a molecular dynamics study, Soft Matter 10 (24) (2014) 4373–4386.
[18] Y. Zheng, X. Gao, L. Jiang, Directional adhesion of superhydrophobic butterfly wings, Soft Matter 3 (2) (2007) 178–182.
[19] K. Liu, L. Jiang, Bio-inspired design of multiscale structures for function integration, Nano Today 6 (2) (2011) 155–175.
[20] J. Yong, Q. Yang, F. Chen, D. Zhang, G. Du, H. Bian, J. Si, X. Hou, Bioinspired superhydrophobic surfaces with directional adhesion, RSC Adv. 4 (16) (2014) 8138–8143.
[21] P. Comanns, G. Buchberger, A. Buchsbaum, R. Baumgartner, A. Kogler, S. Bauer, W. Baumgartner, Directional, passive liquid transport: the Texas horned lizard as a model for a biomimetic liquid diode, J. R. Soc. Interface 12 (109) (2015) 20150415.
[22] A.D. Stroock, R.F. Ismagilov, H.A. Stone, G.M. Whitesides, Fluidic ratchet based on Marangoni–Bénard convection, Langmuir 19 (10) (2003) 4358–4362.
[23] K.-H. Chu, R. Xiao, E.N. Wang, Uni-directional liquid spreading on asymmetric nanostructured surfaces, Nat. Mater. 9 (5) (2010) 413–417.
[24] P. Guo, Y. Zheng, C. Liu, J. Ju, L. Jiang, Directional shedding-off of water on natural/bio-mimetic taper-ratchet array surfaces, Soft Matter 8 (6) (2012) 1770–1775.
[25] A. Cavalli, M.L. Blow, J.M. Yeomans, Modelling unidirectional liquid spreading on slanted microposts, Soft Matter 9 (29) (2013) 6862–6866.
[26] B. Thiria, J. Zhang, Ratcheting fluid with geometric anisotropy, Appl. Phys. Lett. 106 (5) (2015) 054106.
[27] S. Daniel, S. Sircar, J. Gliem, M.K. Chaudhury, Ratcheting motion of liquid drops on gradient surfaces, Langmuir 20 (10) (2004) 4085–4092.
[28] C. Liu, J. Ju, Y. Zheng, L. Jiang, Asymmetric ratchet effect for directional transport of fog drops on static and dynamic butterfly wings, ACS Nano 8 (2) (2014) 1321–1329.
[29] N.T. Chamakos, M.E. Kavousanakis, A.G. Boudouvis, A.G. Papathanasiou, Droplet spreading on rough surfaces: tackling the contact line boundary condition, Phys. Fluids 28 (2) (2016), http://dx.doi.org/10.1063/1.4941577, 022105.
[30] G. Karapetsas, N.T. Chamakos, A.G. Papathanasiou, Efficient modelling of droplet dynamics on complex surfaces, J. Phys.: Condens. Matter 28 (8) (2016) 085101 http://stacks.iop.org/0953-8984/28/i=8/a=085101.
[31] R. Miller, J. Li, M. Bree, G. Loglio, A. Neumann, H. Möhwald, Interfacial relaxation of phospholipid layers at a liquid–liquid interface, Thin Solid Films 327 (1998) 224–227.
[32] Y. Zhang, Z. An, G. Cui, J. Li, Stabilized complex film formed by co-adsorption of $\beta$-lactoglobulin and phospholipids at liquid/liquid interface, Colloids Surf. A: Physicochem. Eng. Aspects 223 (1) (2003) 11–16.
[33] B. Deryaguin, N. Churaev, V. Muller, Surface Forces, Consultants Bureau, New York, 1987.
[34] M.E. Kavousanakis, N.T. Chamakos, A.G. Papathanasiou, Connection of intrinsic wettability and surface topography with the apparent wetting behavior and adhesion properties, J. Phys. Chem. C 119 (27) (2015) 15056–15066, http://dx.doi.org/10.1021/acs.jpcc.5b00718.
[35] B. Dacorogna, P. Marcellini, Implicit Partial Differential Equations, vol. 37, Springer, 1999.
[36] O.C. Zienkiewicz, P. Morice, The Finite Element Method in Engineering Science, vol. 1977, McGraw-Hill, London, 1971.
[37] D. Quéré, Wetting and roughness, Annu. Rev. Mater. Res. 38 (2008) 71–99.
[38] B. Bhushan, Y.C. Jung, K. Koch, Micro-, nano- and hierarchical structures for superhydrophobicity, self-cleaning and low adhesion, Philos. Trans. R. Soc. Lond. A: Math. Phys. Eng. Sci. 367 (1894) (2009) 1631–1672, http://dx.doi.org/10.1098/rsta.2009.0014.
[39] C. Extrand, Retention forces of a liquid slug in a rough capillary tube with symmetric or asymmetric features, Langmuir 23 (4) (2007) 1867–1871.
[40] E. Contraires, J. Teisseire, E. Søndergård, E. Barthel, Wetting against the nap-how asperity inclination determines unidirectional spreading, Soft Matter 12 (28) (2016) 6067–6072.
[41] K.-C. Park, S.S. Chhatre, S. Srinivasan, R.E. Cohen, G.H. McKinley, Optimal design of permeable fiber network structures for fog harvesting, Langmuir 29 (43) (2013) 13269–13277.
[42] S. Daniel, M.K. Chaudhury, P.-G. De Gennes, Vibration-actuated drop motion on surfaces for batch microfluidic processes, Langmuir 21 (9) (2005) 4240–4248.
[43] E.D. Wilkes, O.A. Basaran, Forced oscillations of pendant (sessile) drops, Phys. Fluids (1994–present) 9 (6) (1997) 1512–1528.
[44] F. Celestini, R. Kofman, Vibration of submillimeter-size supported droplets, Phys. Rev. E 73 (4) (2006) 041602.
[45] H. Lamb, Hydrodynamics, Cambridge University Press, 1932.
[46] G. Pashos, G. Kokkoris, A.G. Boudouvis, Minimum energy paths of wetting transitions on grooved surfaces, Langmuir 31 (10) (2015) 3059–3068.
[47] Z.U. Warsi, Fluid Dynamics: Theoretical and Computational Approaches, CRC Press, 2005.